

Fig. 2. Temporal behavior of the ETG mode threshold. Squares gives the UHR trajectory for $f_i = 65$ GHz

To study the small-scale turbulence the movable focusing double antennae set, allowing off equatorial plane plasma X-mode probing with the maximal vertical displacement $y_a = \pm 2$ cm was installed at FT-2 at the high magnetic field side (see Fig. 1). The probing was performed at low power level of 20 mW at frequencies 65, 64 and 57 GHz allowing study of drift wave turbulence at 3-4.5 and 5.5-6.5 cm accordingly. The plasma current was ramped up from 22 kA to 32 kA at the 30th ms of discharge which resulted in the evolution of the plasma parameters profiles and correspondingly to variation of ETG instability threshold and growth rate. The evolution of parameter $(R/L_{Te}) / \max\{0.8R/L_n; (1+Z_{eff}T_e/T_i)(1.33+1.91s/q)(1-1.5r/R_0)\}$ determining, according to [1], the ETG instability threshold provided by the ASTRA code

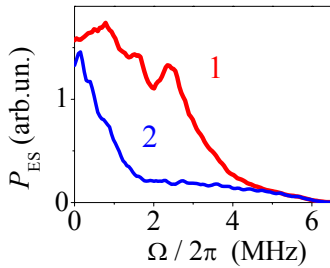


Fig. 3. ES Ω -spectra for $f_i = 65$ GHz (1), 57 GHz (2).

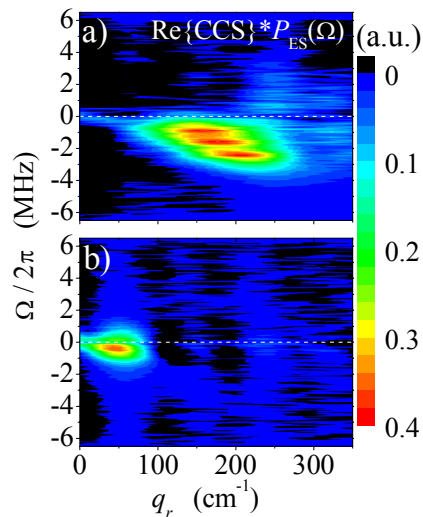


Fig. 4. ES signal spectra for 65 (a) and 57 GHz (b) probing.

modeling is shown in Fig. 2. As it is seen the threshold parameter experiences substantial variation along the trajectory of the 64 GHz probing wave UHR point, being however always higher than unity. The GS2 modelling performed for the selected temporal points have confirmed the positive growth rate value there. From Fig. 2 we could also conclude that the ETG instability is mostly

below the threshold at the plasma edge. Unfortunately a poor accuracy of electron density and temperature determination in this region makes this conclusion not reliable.

The ES frequency spectra $P_{ES}(\Omega)$ measured in the stationary stage of the tokamak discharge (36th ms) at probing frequencies $f_i = 65$ GHz and 57 GHz, corresponding to $r = 3.8$ cm and 5.9 cm are shown in Fig. 3 by curves 1 and 2. As it is seen the frequency shift, as well as structure of the ES spectra, in these cases is very different which corresponds to different origin of

turbulence producing the signal (ETG and TE modes accordingly). To measure the turbulence wavenumber spectrum we applied the correlation ES diagnostics [2]. Two signals at close probing frequencies with difference $|f_2 - f_1| = \{10, 20, \dots, 400\}$ MHz, corresponding to

two slightly separated UHR layers in plasma, where the ES by fluctuations occurs, were measured simultaneously using the asymmetric correlation scheme [2].

The cross-correlation function (CCF) of two ES signals, according to [2] is related to the

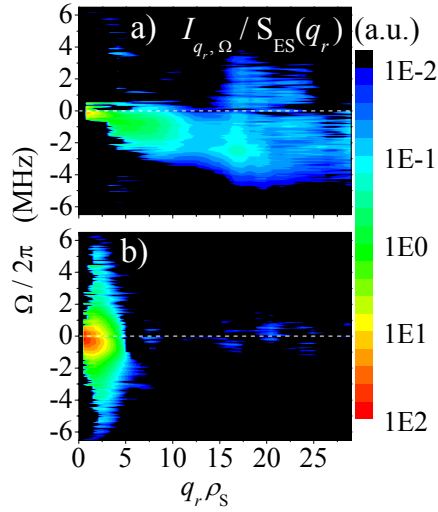


Fig. 5. Turbulence spectra obtained by 65 (a) and 57 GHz (b) probing.

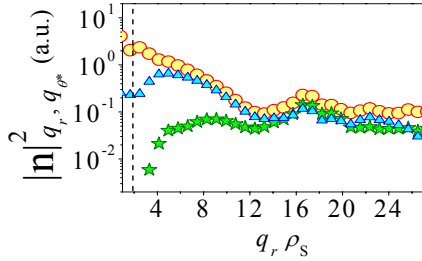


Fig. 6. Turbulence q -spectra at $r = 3.8$ cm, $t = 36$ ms.

it is seen in Fig. 5a, in central zone the turbulence spectrum is very wide both in frequency and in radial wavenumber. It occupies the entire ETG instability domain ($20 > q_r \rho_s > 2$), whereas at the plasma edge the turbulence is exponentially decaying with growing wavenumber, being only observable at $q_r \rho_s < 5$. The ETG turbulence wavenumber spectra obtained from Fig. 5a following values maximal in frequency (yellow points) or cutting at 2 and 4 MHz (blue and green points, correspondingly) are shown in Fig. 6. They demonstrate rather weak (less than two orders of magnitude) spectrum variation with growing wavenumber and thus confirm the above conclusions. The temporal behaviour of the ETG turbulence density perturbation $\delta n \sim \int |n|^2_{q_r, \Omega} dq_r d\Omega$

turbulence spectrum $|n|^2_{q_r, \Omega}$ by equation

$$CCF_{\Omega}(f_1, f_2) = \int I_{q_r, \Omega} \exp\{iq_r [(f_1 - f_2) \partial x_{UH} / \partial f]\} dq_r,$$

where the ES spectrum $I_{q_r, \Omega} = |n|^2_{q_r, \Omega} S_{ES}(q_r)$ and $S_{ES}(q_r)$

is ES efficiency [2]. The determined dependence of the normalized CCF of two ES signals on $f_2 - f_1$ (proportional to the corresponding UHR spatial separation) was Fourier transformed and multiplied by the ES homodyne spectra (Fig. 3) to get the ES spectra $I_{q_r, \Omega}$ shown in Fig. 4. As it

is seen, the wavenumber of fluctuations contributing to the ES signal in the central zone and at the edge differs by a factor of 3-4 indicating different physical origin of turbulence in these regions.

The turbulence spectra $|n|^2_{q_r, \Omega}$ can be obtained from ES spectra of Fig. 4 after accounting for the strong ES efficiency dependence on fluctuation wavenumber [2]. As

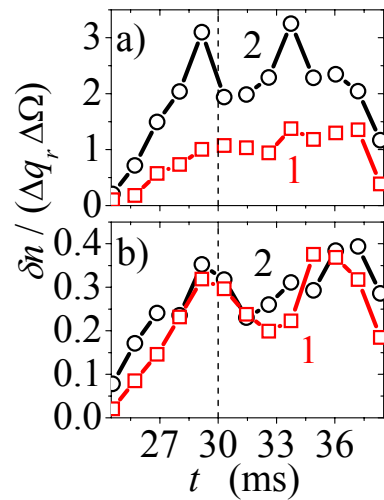


Fig. 7. Integrated turbulent density perturbation for 65 GHz (1) and 64 GHz (2) probing.

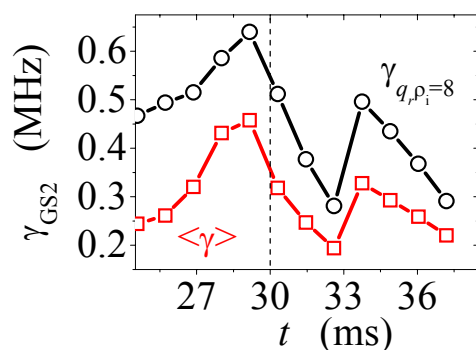


Fig. 8. The growth rate behavior calculated with the GS2 code for linear modes.

integrated over all the wavenumber and frequency domain where it was measured ($\Delta q_r \rho_s = [2..16]$; $\Delta \Omega / 2\pi = [-3.7 .. -0.4]$ MHz) is shown in Fig. 7a for probing frequencies 65 and 64 GHz. As it is seen, in both cases the turbulent density perturbation is growing at $t < 29.2$ ms and decaying at $t > 33.7$ ms, whereas at $29.2 \text{ ms} < t < 33.7 \text{ ms}$ its behavior is non monotonous. Similar evolution is typical also for the small-scale, high frequency component

($\Delta q_r \rho_s = [5..16]$; $\Delta \Omega / 2\pi = [-3.7 .. -1.8]$ MHz), as it is seen in Fig. 7b.

It is important to note that this behavior well correlates with the ETG mode instability growth rate evolution, as provided by the GS2 code [9]. The corresponding dependencies are plotted on Fig. 8 for the growth rate $\langle \gamma \rangle$ averaged over the interval $0.1 < q_r \rho_i < 10$ (squares) and the growth rate calculated for $q_r \rho_i = 8$ (circles).

Conclusions

Summarizing the paper results it is worth to underline that measurements of the small-scale turbulence component performed in the gradient FT-2 discharge zone where the ETG mode is definitely unstable both according to the threshold conditions [1] and to the GS2 computation have resulted in observation of wide radial wavenumber spectra at $2 < q_r \rho_s < 16$. It is shown that temporal evolution of the turbulence level in the dynamic CRU discharge follows the behavior of the ETG instability growth rate as provided by the GS2 code, thus giving additional confirmation of its ETG mode origin.

Financial support of RFBR Grants, 08-02-00989, 07-02-00895, 08-02-00610, Centre-of-Excellence grant 047.018.002 and "Russian Science Support Foundation" is acknowledged. The facilities of CSC Finnish IT Center for Science have been used for this work.

1. Jenko F., Dorland W., Kotschenreuther M. and Rogers B.N. 2000 *Phys. Plasmas* **7** 1904
2. E.Z. Gusakov, A.D. Gurchenko, A.B. Altukhov et al. 2006 *Plasma Phys. Control. Fusion* **48** A371
3. A.D. Gurchenko, E.Z. Gusakov, A.B. Altukhov et al. 2007 *Nucl. Fusion* **47** 245
4. T.L. Rhodes, W.A. Peebles, J.C. DeBoo et al. 2007 *Plasma Phys. Control. Fusion* **49** B183
5. E. Mazzucato, D.R. Smith, R.E. Bell et al. 2008 *Phys. Rev. Lett.* **101** 075001
6. E. Mazzucato, et al. http://www-pub.iaea.org/MTCD/Meetings/FEC2008/ex_10-2ra.pdf
7. E. Gusakov, et al. http://www-pub.iaea.org/MTCD/Meetings/FEC2008/ex_10-2rb.pdf
8. A.D. Gurchenko, et al., 35 *EPS Conf. on Plasma Physics, Hersonissos, 2008*, ECA Vol.32D, O-4.046.
9. M. Kotschenreuther, G. Rewoldt, W.M. Tang, *Comp. Phys. Comm.* **88**, 128 (1995)